

## Supporting information for

# Reverse Water-Gas Shift Reaction Catalyzed by Diatomic Rhodium Anions

Yun-Zhu Liu,<sup>abc</sup> Jiao-Jiao Chen,<sup>ac</sup> Li-Hui Mou,<sup>abc</sup> Qing-Yu Liu,<sup>ac</sup> Zi-Yu Li,<sup>ac</sup> Xiao-Na Li,<sup>\*ac</sup> and  
Sheng-Gui He<sup>\*abc</sup>

<sup>a</sup> State Key Laboratory for Structural Chemistry of Unstable and Stable Species, Institute of  
Chemistry, Chinese Academy of Sciences, Beijing 100190, China

<sup>b</sup> University of Chinese Academy of Sciences, Beijing 100049, China

<sup>c</sup> Beijing National Laboratory for Molecular Sciences and CAS Research/Education Center of  
Excellence in Molecular Sciences, Beijing 100190, China

### Corresponding Author

\* Xiao-Na Li, E-mail: [lxn@iccas.ac.cn](mailto:lxn@iccas.ac.cn)

\* Sheng-Gui He, E-mail: [shengguihe@iccas.ac.cn](mailto:shengguihe@iccas.ac.cn)

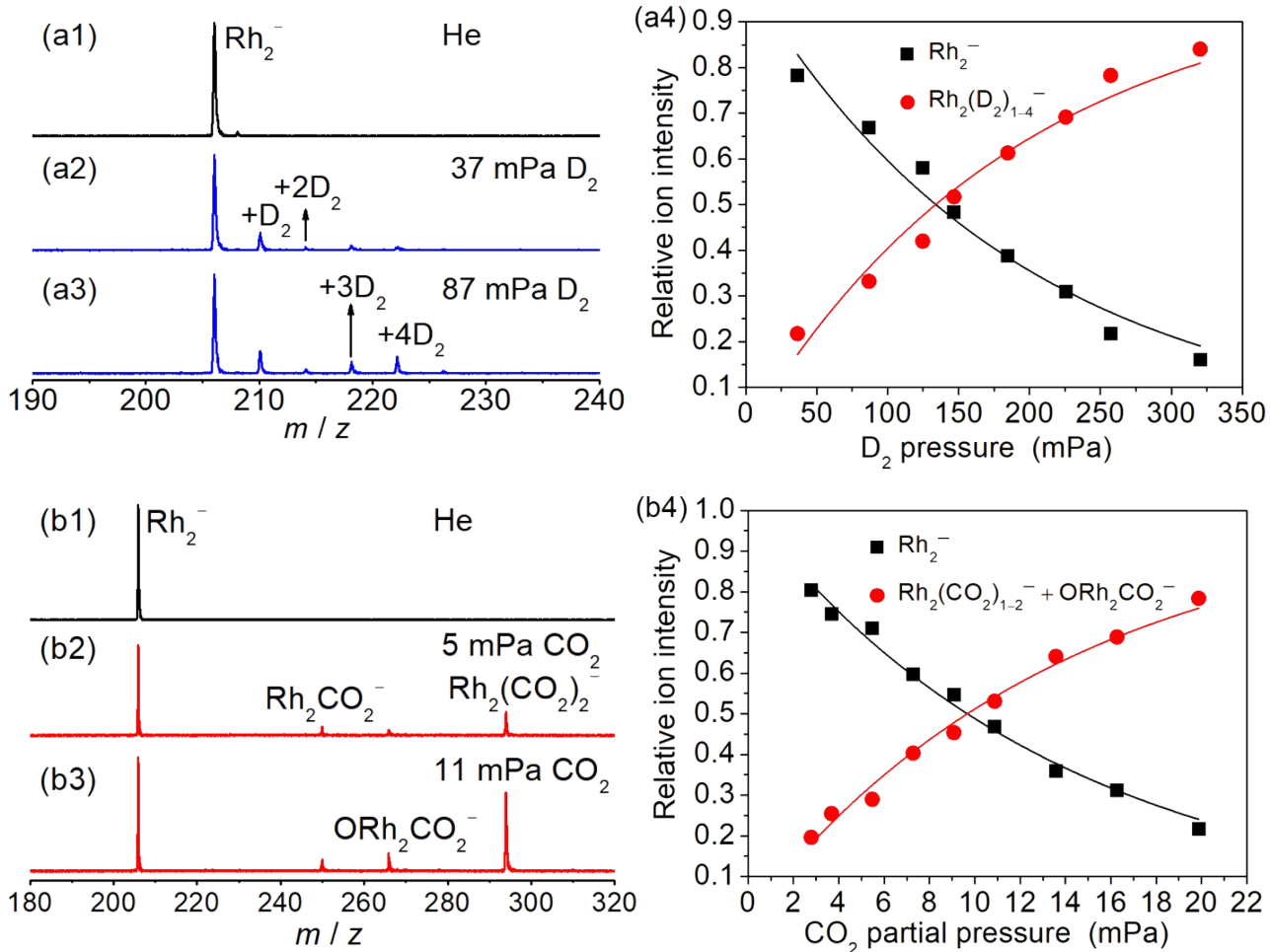


**Fig. S1** The time-of-flight (TOF) mass spectra for the reactions of mass-selected  $\text{Rh}_2^-$  anions with  $\text{D}_2$  (a1-a3) and  $\text{CO}_2$  (b1-b3) are shown and reactant pressures are given in mPa ( $= 10^{-3}$  Pa). Variations of ion intensities with respect to the reactant pressures on the reactions of  $\text{Rh}_2^-$  with  $\text{D}_2$  and  $\text{CO}_2$  are presented in a4 and b4, respectively. The solid lines are fitted to the experimental data points by the least-square procedure. The determined rate constants are given in Table S1.

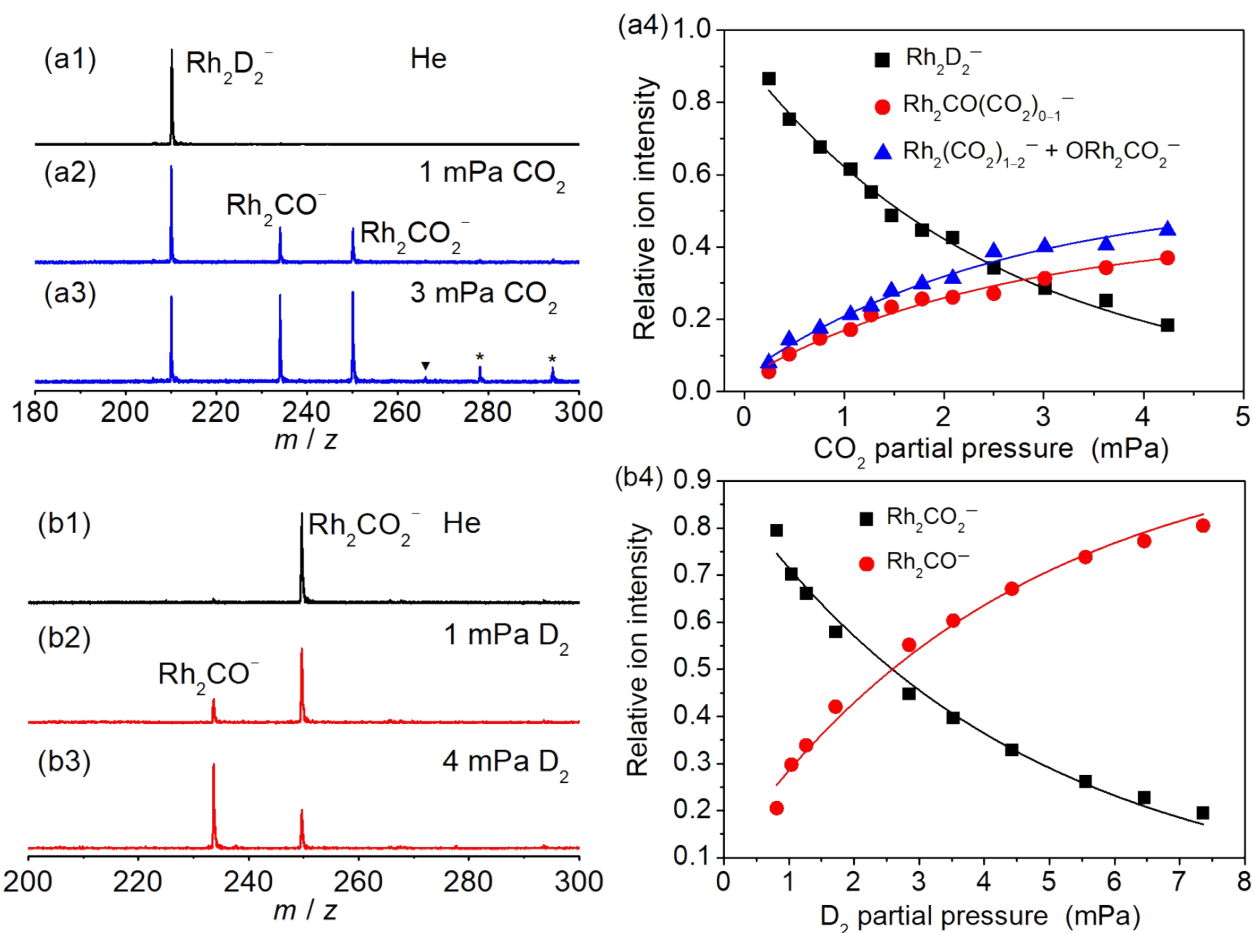


**Fig. S2** The TOF mass spectra for the reactions of mass-selected products  $\text{Rh}_2\text{D}_2^-$  and  $\text{Rh}_2\text{CO}_2^-$  generated in LIT1 with  $\text{CO}_2$  (a1-a3) and  $\text{D}_2$  (b1-b3) in LIT2, respectively. The reactant pressures are shown in mPa ( $= 10^{-3}$  Pa). The weak signal marked with a triangle in panel a3 is  $\text{ORh}_2\text{CO}_2^-$  due to the reduction of  $\text{CO}_2$  by  $\text{Rh}_2\text{CO}_2^-$  ( $\text{Rh}_2\text{CO}_2^- + \text{CO}_2 \rightarrow \text{ORh}_2\text{CO}_2^- + \text{CO}$ ). The signals marked with asterisks are  $\text{Rh}_2\text{CO}(\text{CO}_2)^-$  and  $\text{Rh}_2(\text{CO}_2)_2^-$ , respectively, corresponding with the adsorption of  $\text{CO}_2$  on  $\text{Rh}_2\text{CO}^-$  and  $\text{Rh}_2\text{CO}_2^-$ . Variations of ion intensities with respect to the reactant pressures on the reactions of  $\text{Rh}_2\text{D}_2^-$  with  $\text{CO}_2$  and  $\text{Rh}_2\text{CO}_2^-$  with  $\text{D}_2$  are presented in a4 and b4, respectively. The solid lines are fitted to the experimental data points by the least-square procedure. The determined rate constants are given in Table S1.

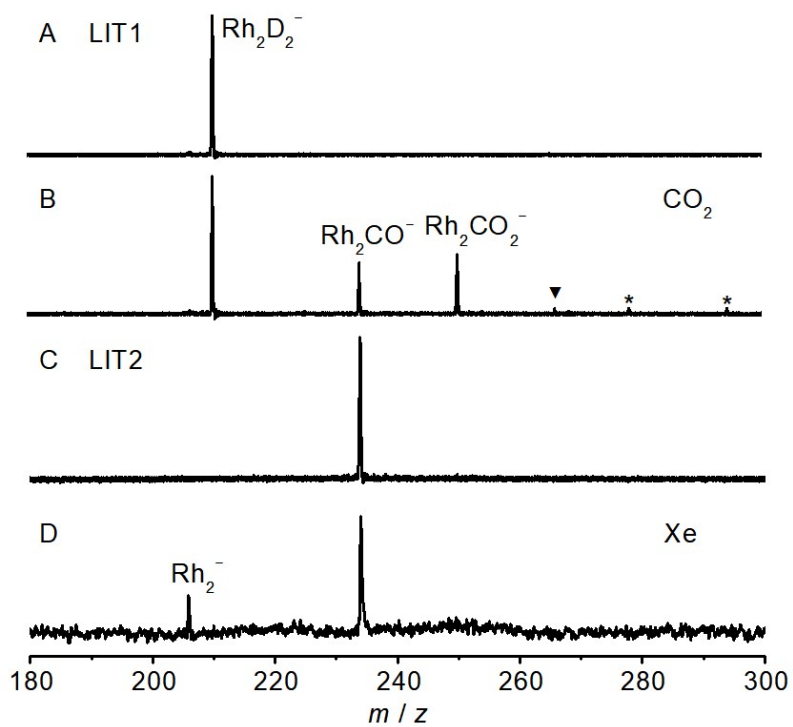


**Fig. S3** The TOF mass spectra for the reactions of mass-selected  $\text{Rh}_2\text{D}_2^-$  (A) anions with  $\text{CO}_2$  (B) in LIT1. Collision-induced dissociation spectra of mass-selected  $\text{Rh}_2\text{CO}^-$  with 50 mPa Xe in the collision cell (LIT2). The center-of-mass collision energy  $E_c$  is roughly estimated to be about 5.38 eV.

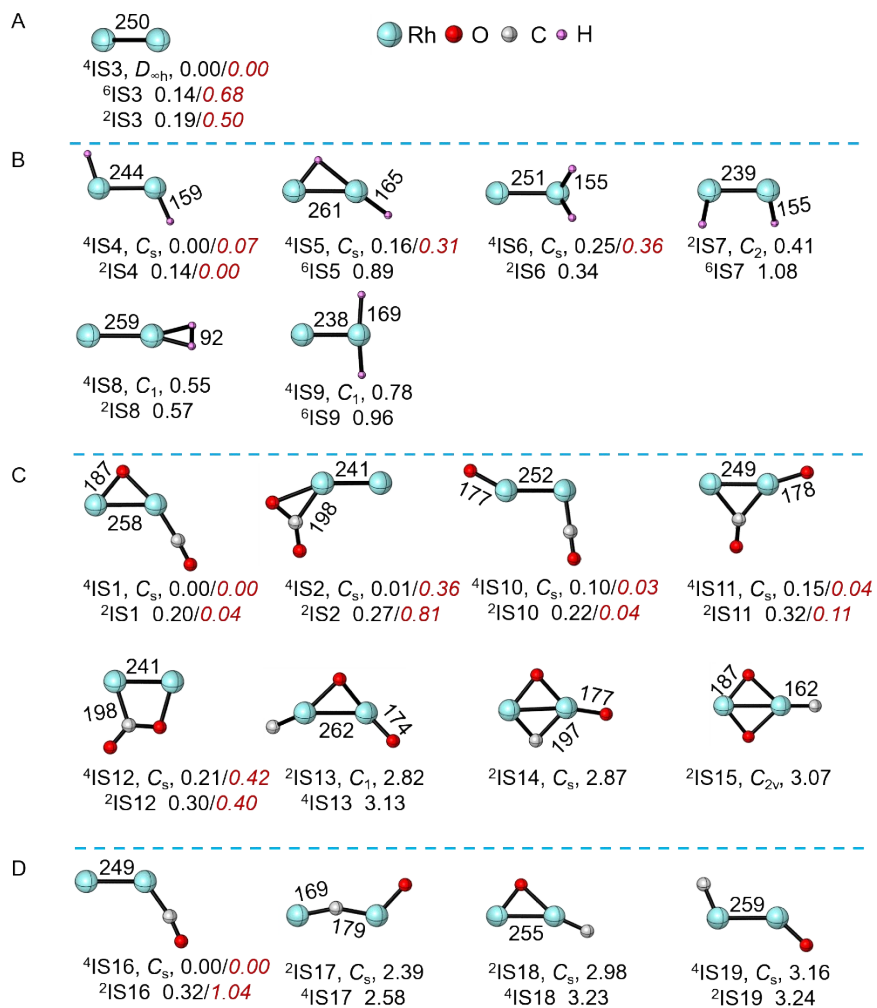


**Fig. S4** The calculated low-lying isomers of  $\text{Rh}_2^-$  (A),  $\text{Rh}_2\text{H}_2^-$  (B),  $\text{Rh}_2\text{CO}_2^-$  (C), and  $\text{Rh}_2\text{CO}^-$  (D).

The relative energies ( $\Delta H_0$ , in eV) with respect to the lowest-lying isomer are given at the B3LYP and the RCCSD(T) (the red values in italic) levels of theory.

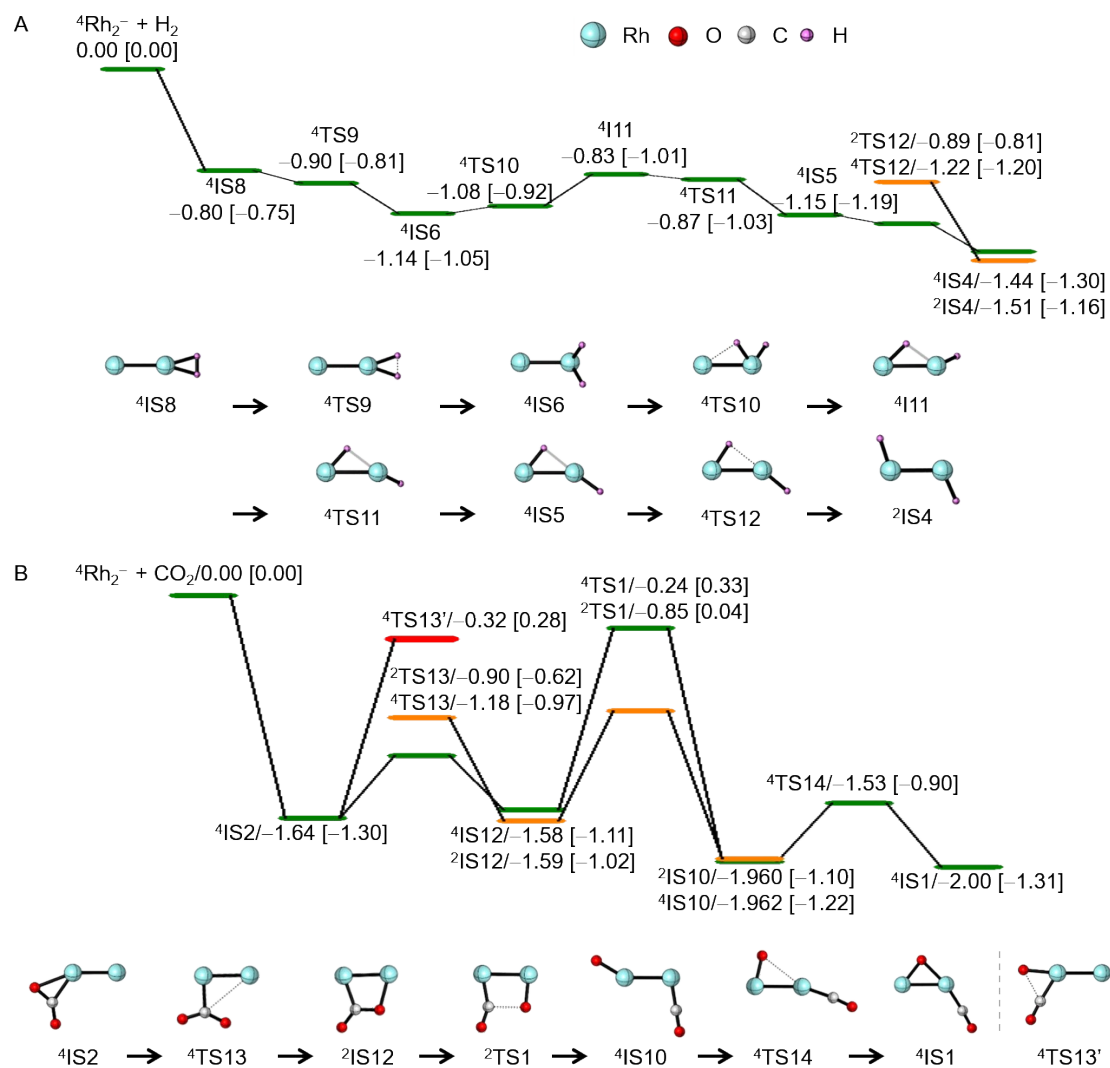


**Fig. S5** The potential energy profiles for the reaction of  $\text{Rh}_2^-$  with  $\text{H}_2$  (A) and  $\text{CO}_2$  (B). The zero-point vibration corrected energies ( $\Delta H_0$ , in eV) with respect to the separated reactants are given at the RCCSD(T) and the B3LYP (in square brackets) levels of theory. The superscripts represent the spin multiplicities.

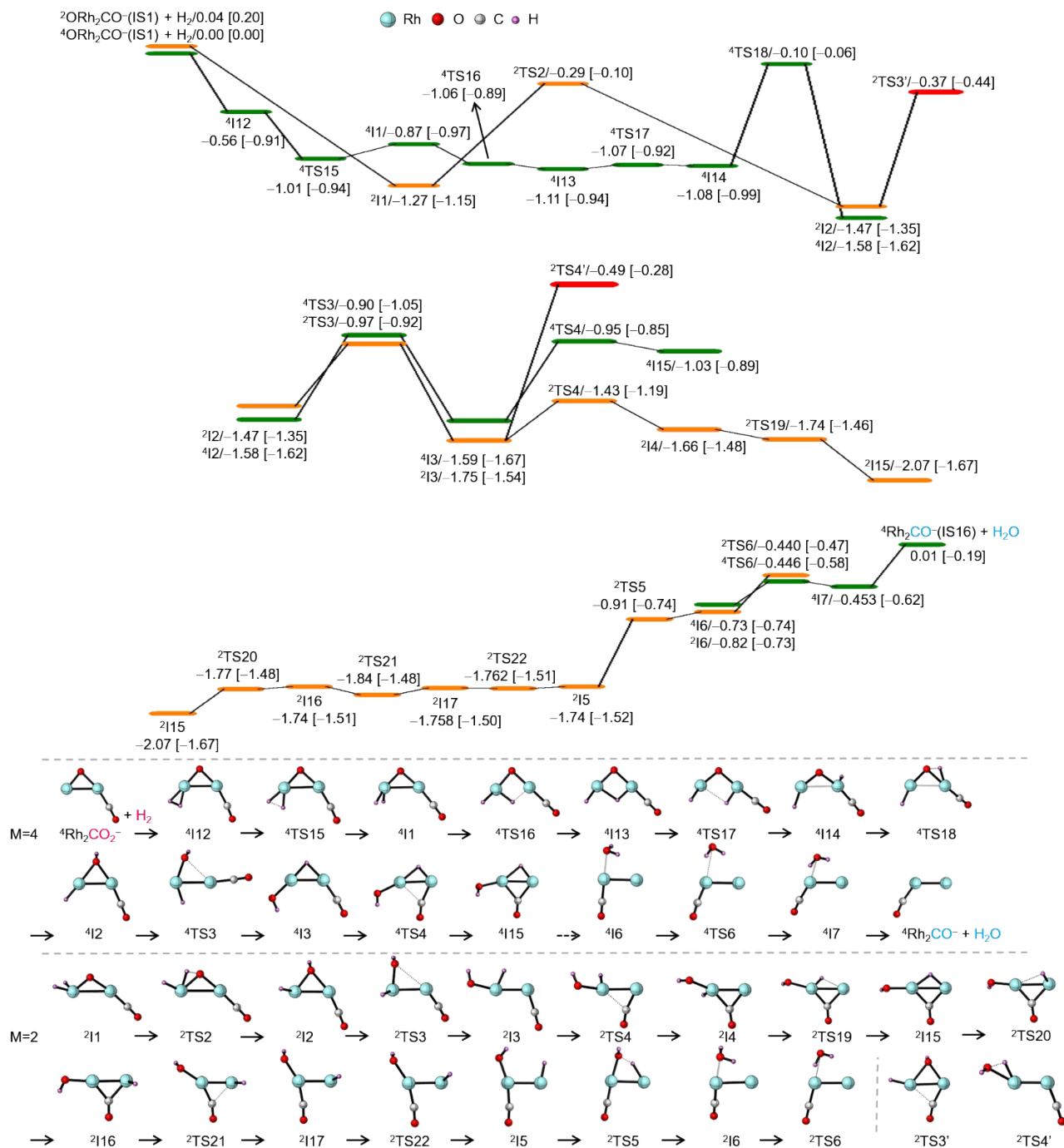


**Fig. S6** The potential energy profiles for the reaction of  $\text{ORh}_2\text{CO}^-$  with  $\text{H}_2$ . The zero-point vibration corrected energies ( $\Delta H_0$ , in eV) with respect to the separated reactants ( ${}^4\text{ORh}_2\text{CO}^- + \text{H}_2$ ) are given at the RCCSD(T) and the B3LYP (in square brackets) levels of theory. The superscripts represent the spin multiplicities.

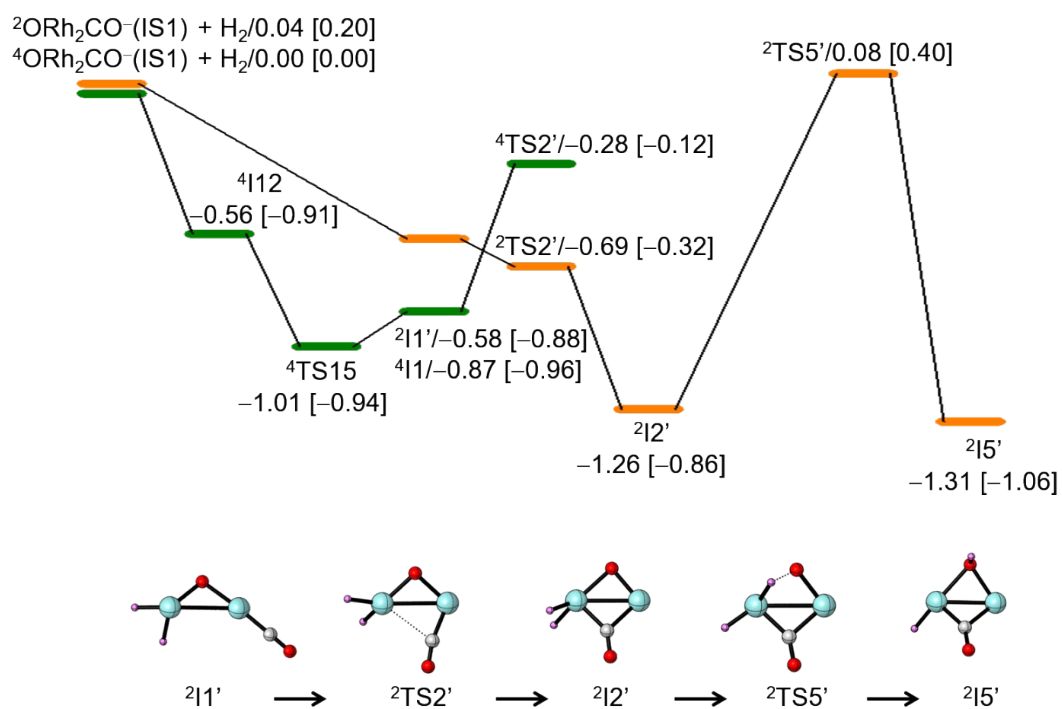


**Fig. S7** The potential energy profile for the reaction of  $\text{ORh}_2\text{CO}^-$  with  $\text{H}_2$ . The zero-point vibration corrected energies ( $\Delta H_0$ , in eV) with respect to the separated reactants ( ${}^4\text{ORh}_2\text{CO}^- + \text{H}_2$ ) are given at the RCCSD(T) and the B3LYP (in square brackets) levels of theory. The superscripts represent the spin multiplicities.



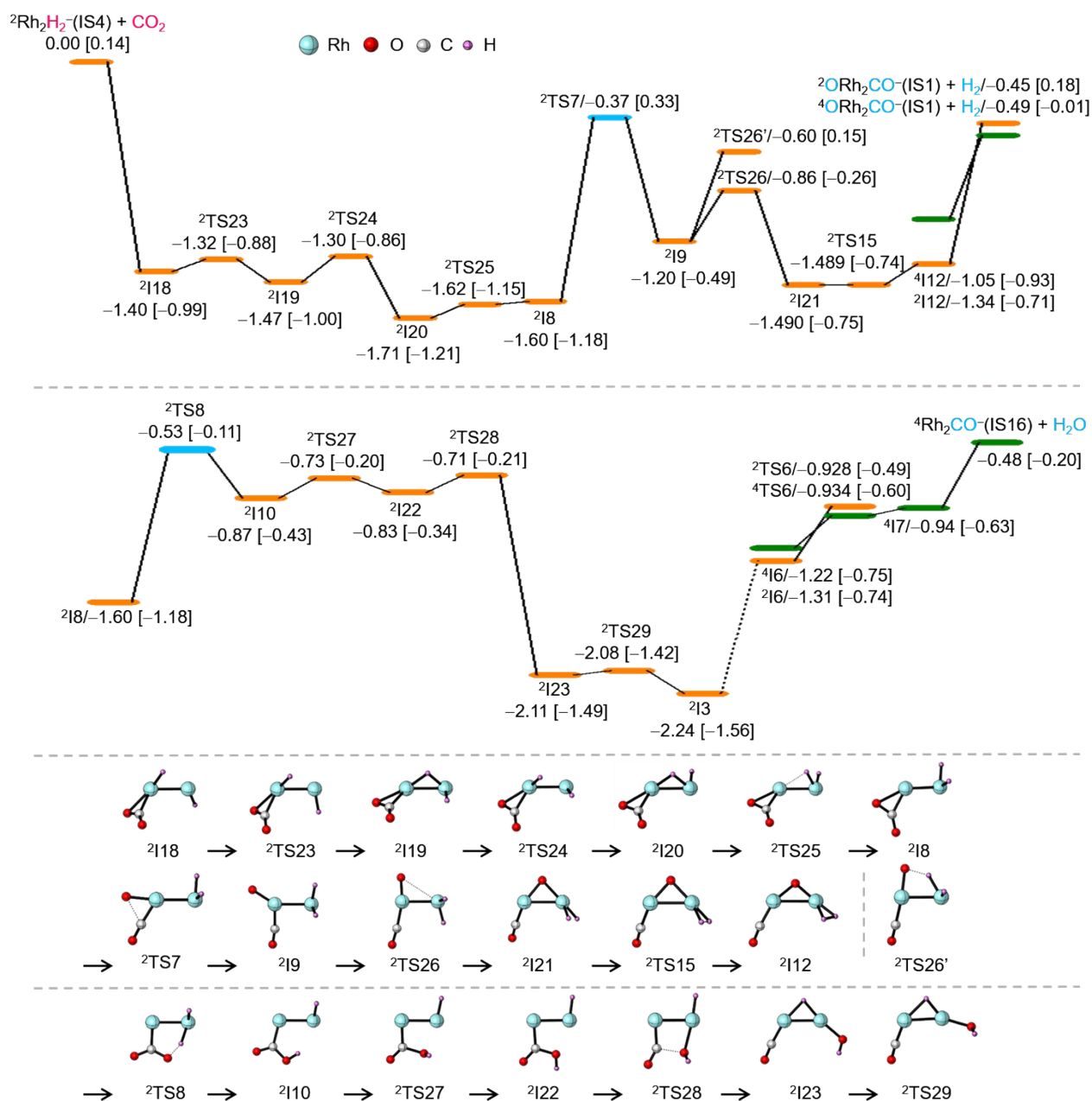


**Fig. S8** The potential energy profiles for the reaction of  $\text{Rh}_2\text{H}_2^-$  with  $\text{CO}_2$ . The zero-point vibration corrected energies ( $\Delta H_0$ , in eV) with respect to the separated reactants ( ${}^2\text{Rh}_2\text{H}_2^- + \text{CO}_2$ ) are given at the RCCSD(T) and the B3LYP (in square brackets) levels of theory. The superscripts represent the spin multiplicities.

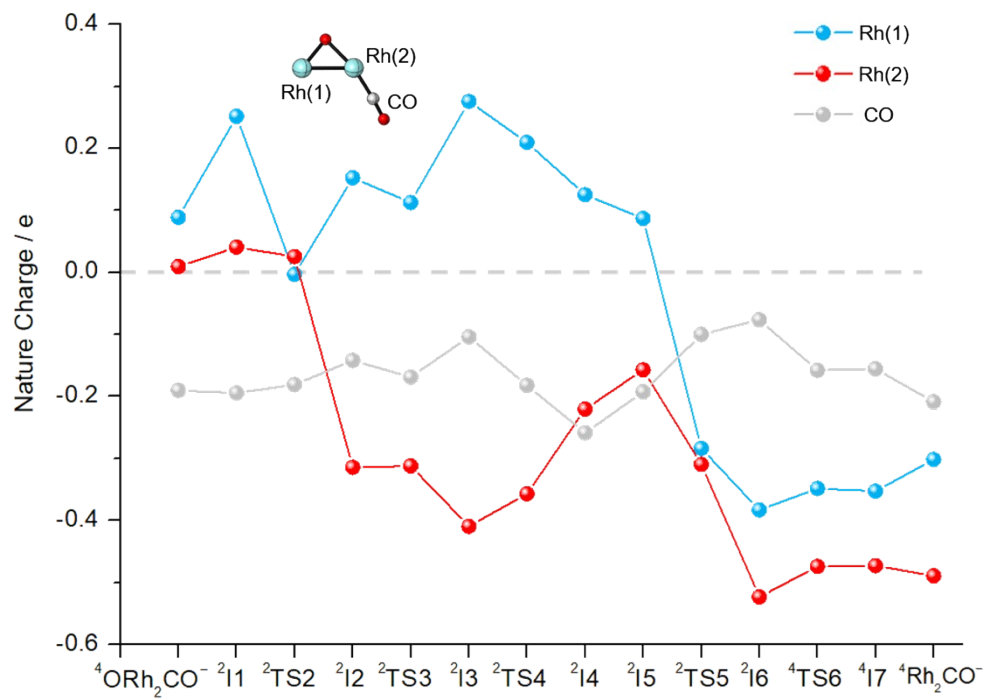


**Fig. S9** Natural charges on the Rh(1) and Rh(2) atoms and the CO moiety along with the reaction coordinates of  $\text{ORh}_2\text{CO}^-$  ( ${}^4\text{IS1}$ ) +  $\text{H}_2$  (Fig. 3).

**Table S1.** DFT calculated and experimental bond dissociation enthalpies (in eV) of Rh–Rh, Rh–H, Rh–C, Rh–O, O–CO, C–O, H–H, O–H, and H–OH as well as vertical detachment energies (VDE in eV) of Rh<sub>2</sub><sup>-</sup>.

	<i>D</i> (A–B)									VDE
	Rh–Rh	Rh–H	Rh–C	Rh–O	O–CO	C–O	H–H	O–H	H–OH	Rh <sub>2</sub> <sup>-</sup>
Exp <sup>1,2</sup>	2.406	2.420	5.973	4.159	5.477	11.120	4.478	4.417	5.113	1.65
M06L	2.931	3.001	6.060	4.354	5.774	10.928	4.215	4.191	4.749	1.092
BPW91	2.813	2.963	6.314	4.638	5.917	11.185	4.312	4.384	4.901	1.334
BLYP	2.919	3.007	6.175	4.664	5.723	11.119	4.469	4.440	4.905	1.260
BP86	3.012	3.146	6.487	4.808	6.014	11.367	4.563	4.583	5.077	1.517
TPSS	3.138	3.335	6.222	4.594	5.576	10.779	4.619	4.319	4.866	1.222
PBE	3.083	3.013	6.564	4.873	6.121	11.425	4.268	4.446	4.965	1.361
BPBE	2.829	2.961	6.339	4.653	5.935	11.195	4.288	4.376	4.898	1.323
<b>B3LYP</b>	<b>1.736</b>	<b>2.862</b>	<b>5.303</b>	<b>3.799</b>	<b>5.441</b>	<b>10.803</b>	<b>4.497</b>	<b>4.364</b>	<b>4.884</b>	<b>1.472</b>
B1LYP	1.559	2.756	4.932	3.466	5.229	10.558	4.442	4.260	4.779	1.164
X3LYP	1.727	2.846	5.251	3.755	5.437	10.794	4.473	4.353	4.879	1.430
B1B95	1.696	2.823	5.351	3.720	5.522	10.902	4.379	4.264	4.914	1.103
B3P86	1.812	2.992	5.613	3.967	5.745	11.061	4.575	4.506	5.054	1.986
B3PW91	1.651	2.822	5.401	3.760	5.576	10.819	4.371	4.307	4.873	1.240
PBE1PBE	1.630	2.752	5.291	3.634	5.590	10.810	4.247	4.255	4.828	1.425
M062X	1.605	2.742	5.076	3.435	5.317	10.969	4.405	4.300	4.860	1.064

**Table S2.** Total rate constants ( $k_1$ , in unit of  $10^{-10}$  cm<sup>3</sup> molecule<sup>-1</sup> s<sup>-1</sup>), and reaction efficiency ( $\Phi$ ) for the reactions  $\text{Rh}_2^- + \text{D}_2$ ,  $\text{Rh}_2\text{D}_2^- + \text{CO}_2$ ,  $\text{Rh}_2^- + \text{CO}_2$ , and  $\text{Rh}_2\text{CO}_2^- + \text{D}_2$ .

reactions	products	$k_1$	$\Phi^a$ (%)
$\text{Rh}_2^- + \text{D}_2$	$\text{Rh}_2\text{D}_2^-$	$0.013 \pm 0.003$	$0.07 \pm 0.01$
$\text{Rh}_2\text{D}_2^- + \text{CO}_2$	$\text{Rh}_2\text{CO}^- + \text{D}_2\text{O}$	$8.1 \pm 1.7$	$77 \pm 16$
	$\text{Rh}_2\text{CO}_2^- + \text{D}_2$		
$\text{Rh}_2^- + \text{CO}_2$	$\text{Rh}_2\text{CO}_2^-$	$0.33 \pm 0.07$	$3.2 \pm 0.7$
$\text{Rh}_2\text{CO}_2^- + \text{D}_2$	$\text{Rh}_2\text{CO}^- + \text{D}_2\text{O}$	$5.1 \pm 1.1$	$25 \pm 5.3$

<sup>a</sup>Reaction efficiency defined as  $\Phi = k_1/k_{\text{calc}}$ , in which  $k_{\text{calc}}$  is the theoretical rate of collision that is calculated with the surface charge capture (SCC) theory.<sup>3</sup>

## References

- 1 M. R. Beltrán, F. Buendía Zamudio, V. Chauhan, P. Sen, H. Wang, Y. J. Ko and K. Bowen, *Eur. Phy. J. D* 2013, **67**, 63.
- 2 Y. R. Luo, *Comprehensive Handbook of Chemical Bond Energies*; CRC Press: Boca Raton, FL, 2007.
- 3 G. Kummerlöwe and M. K. Beyer, *Int. J. Mass Spectrom.*, 2005, **244**, 84–90.